Title

Mechanical design and fabrication of the VHF-gun, the Berkeley normal-conducting continuous-wave high-brightness electron source

Journal

Review of Scientific Instruments, 87(2)

ISSN

0034-6748

Authors

Wells, RP

Ghiorso, W

Staples, J

et al.

Publication Date

2016-02-01

DOI

10.1063/1.4941836

Peer reviewed

Mechanical design and fabrication of the VHF−Gun, the Berkeley normal-conducting continuous-wave high-brightness electron source[a)]

R. P. Wells,[1, b)] W. Ghiorso,[1] J. Staples,[1] T. M. Huang,[2, 1] F. Sannibale,[1] and T. D. Kramasz[1]
[1)] *Lawrence Berkeley National Laboratory, Berkeley CA, 94720, USA*
[2)] *Institute of High Energy Physiscs, Beijing, China*

(Dated: 22 January 2016)

A high repetition rate, MHz-class, high-brightness electron source is a key element in future high-repetition-rate x-ray FEL-based light sources. The VHF-Gun, a novel low frequency radio-frequency gun, is the Lawrence Berkeley National Laboratory (LBNL) response to that need. The gun design is based on a normal conducting, single cell cavity resonating at 186 MHz in the VHF band, and capable of continuous wave operation while still delivering the high accelerating fields at the cathode required for the high brightness performance. The VHF-Gun was fabricated and successfully commissioned in the framework of the Advanced Photo-injector EXperiment (APEX), an injector built at LBNL to demonstrate the capability of the gun to deliver the required beam quality. The basis for the selection of the VHF-Gun technology, novel design features and fabrication techniques are described.

PACS numbers: 29.25.Bx, 29.27.Bd, 29.27.Eg, 41.60.Cr

I. INTRODUCTION

In the last decade, a number of proposals for MHz-class repetition rate x-ray free electron lasers (FELs) have been developed[1–4] in response to the pressing needs of the scientific community[5]. To meet this need, the Linear Coherent Light Source-II (LCLS-II) has been funded and is now in construction at SLAC[6]. An electron gun capable of delivering the required beam quality at a high repetition rate[7] was identified as a critical missing element for this next generation of light source. In response, Lawrence Berkeley National Laboratory (LBNL) developed the VHF-Gun, a novel electron source designed and optimized for the achievement of the required goals.

The VHF-Gun, based on a normal-conducting single-cell radio-frequency (RF) cavity resonating at 186 MHz in the VHF band (30 to 300 MHz), is capable of continuous wave (CW) operation while still delivering the high accelerating fields at the cathode required for high brightness performance[8–10]. The electrons are generated by photoemission from a laser illuminated high quantum efficiency (QE) cathode located inside the gun cavity. A picture of the gun just after installation in the Advanced Photo-injector EXperiment (APEX) at LBNL, in spring 2011, is shown in Fig. 1. APEX includes a 20 MeV linac and a complete suite of electron beam diagnostics, and was funded to demonstrate the capability of the VHF-Gun to deliver the required beam quality when integrated in a real injector scheme[11,12].

The RF design and performance results of the VHF-Gun and of APEX beam are reported elsewhere[8–12]. This paper is focused on the description of the mechanical design and the technological choices used to fabricate the VHF-Gun.

II. DESIGN GOALS

The main goal that guided the development of the VHF-Gun, was to produce a reliable CW, high repetition rate (MHz-class) electron source with evenly spaced bunches and high brightness. The final quantitative design goals for the VHF gun are shown in the Table I.

The choice of a VHF-band cavity has its origins in three factors that effectively address most of the requirements in the Table. Firstly, for a fixed energy gain, the wall power density is a strong function of f_{RF}, the cavity resonant frequency[15]: $P_{wall} \propto f_{RF}^{5/2}$. This allows operation with RF power density values on the cavity walls that are compatible with CW operation, while preserving high accelerating fields and high beam energy. Secondly, the relatively long wavelength allows high vacuum conductance slots to be opened in the cavity wall without causing a significant perturbation to the RF performance[16–18]. Thirdly, similarly to the case of DC guns, the acceleration potential is effectively constant over the time scale of interest ($<\sim$ 60 ps) while VHF operation provides a significant enhancement to the voltage breakdown limit, relative to DC conditions.

To operate in a user facility, the gun must be capable of continuous operation over periods of a week or longer with better than 99% availability. The guiding principal was to utilize proven technology and a conservative design approach. To maintain system design flexibility, the frequency of the VHF Gun was selected to be compatible with either of the superconducting linac RF technologies (7-th and 8-th subharmonic of 1.3 GHz and 1.5 GHz respectively) dominant at the time.

In order to operate at the required charge per bunch of several hundred pC at MHz repetition rate[7], the use

[a)] Work supported by the Director of the Office of Science of the US Department of Energy under Contract no. DEAC02-05CH11231
[b)] rpwells@lbl.gov

TABLE I. List of the relevant VHF Cavity Design Parameters and Achieved Results

Parameter	**Design Value**	**Measured Value**	**Units**
Operation Mode	CW	CW	
Accelerating Gap	40	40	mm
Frequency	186	186	MHz
Nominal Gap Voltage	0.75	> 0.85	MV
Q_0	31600	30040	
Electric Field at Cathode at 0.75 MV	19.5	>22	MV/m
Peak Surface Field at 0.75 MV	24.1	not measured	MV/m
RF Power for 0.75 MV	< 100	~ 85	kW
Peak Wall Power Density at 0.75 MV	25	not measured	W/cm^2
Operation Pressure at 0.75 MV	10^{-10}-10^{-9}	$\sim 5 \times 10^{-10}$	Torr
Dark current at 0.75 MV	< 1	$< 10^{-3}$	μA
Cavity Internal Diameter	0.694	0.694	m
Cavity Length	0.35	0.35	m

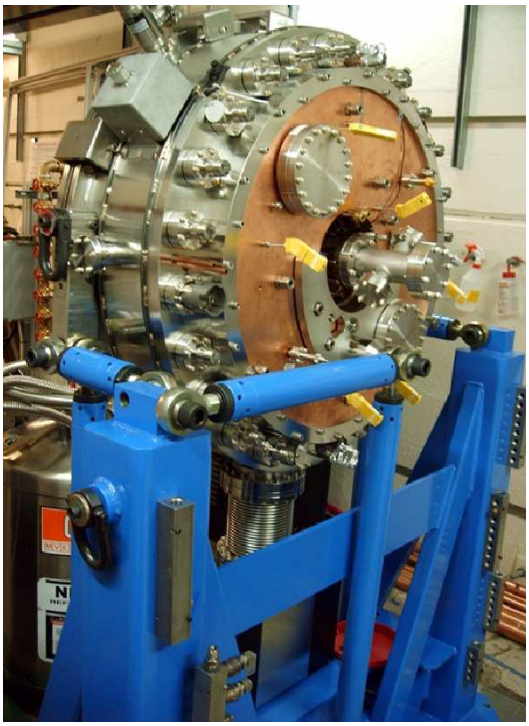

FIG. 1. The VHF-Gun just installed in the shielded area in April 2011.

of high quantum efficiency (QE$\gtrsim 10^{-2}$) photocathodes is necessary for realistic drive laser power levels. Robust but low efficiency metal cathodes (QE$\sim 10^{-5}$) are not practical due to the large laser power demands. Semiconductor materials used in combination with (commercially available) lasers delivering tens of watts of power in the infrared (to be converted into the green or UV wavelenths, depending on the cathode being used) are the only practical alternative. Semiconductors such as Cs_2Te or multi-alkali antimonides offer very high initial QEs of $\sim 10^{-1}$ but are very delicate and reactive. Operating such cathodes with acceptable QE lifetimes requires extremely low vacuum pressures as shown in Table I. A detailed review of cathodes and of their properties can be found elsewhere[13].

Space charge can increase the beam emittance and hence affect the photoemission brightness[7]. To counter space charge in the VHF-Gun, a gradient at the cathode of ∼20 MV/m and a total accelerating voltage of 750 kV were conservatively selected.

The shape of the cavity was tailored to produce the desired gradient and total accelerating voltage with less than 100 kW of input power. Concurrently, multipactoring was minimized over a significant range of input power while maintaining surface power densities below 30 W/cm^2. See reference[14] for more details. A drawing of the VHF-Gun in cross-section is provided in Fig. 2 for reference, and a cross-section of the CAD model of the gun with some of the key design elements in evidence is shown in Fig. 3.

III. KEY DESIGN FEATURES

The VHF Gun design represents a significant extension to some features found in previous RF accelerating cavities. To maintain a 10^{-10} Torr pressure during full power operation, see Fig. 3, an annular pumping plenum

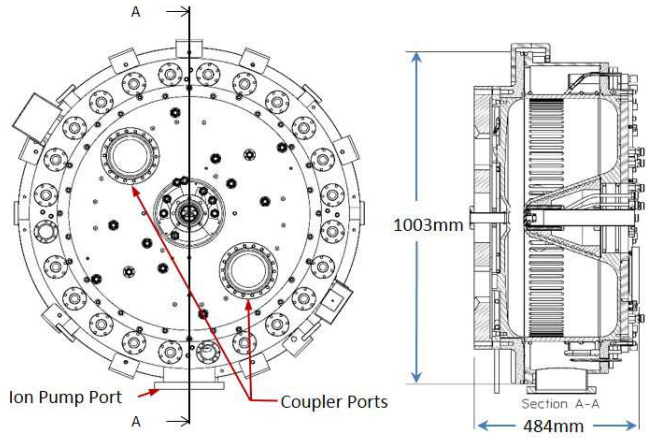

FIG. 2. VHF-Gun, cathode end view and cross section.

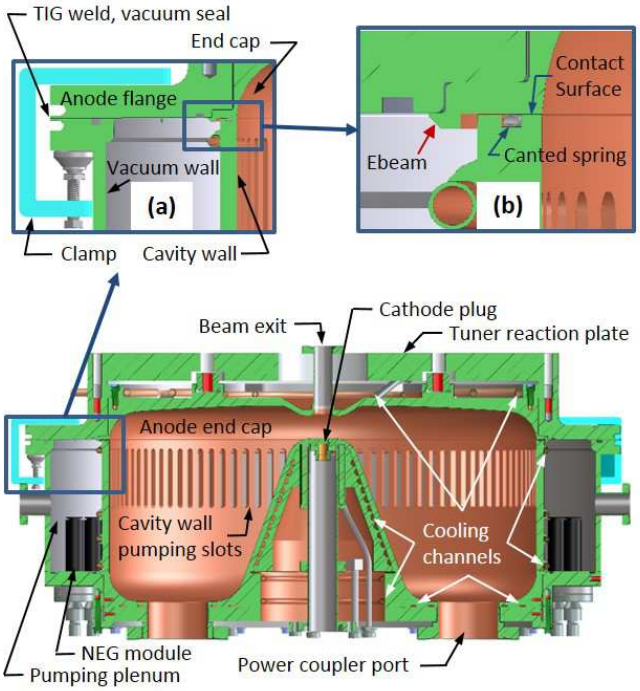

FIG. 3. VHF-Gun in cross-section with detail insets.

surrounds the cavity wall. The wall contains one hundred and four pumping slots that provide a large gas flow conductance to up to twenty-four 400 l/s NEG pumps that protrude into the plenum. The NEG modules are horizontally offset with respect to the cavity wall slots to avoid particulates, that could detach from the pumps, from entering the cavity by gravity.

Commercial, Conflat flange mounted NEG modules (D-400 from SAES) are employed to allow easy replacement. All NEG modules were initially activated 3 times in a separate vacuum chamber before being installed in the gun, following the established procedure for eliminating particulates from the NEG modules[19]. In addition, one 300 l/s ion pump is attached to the vacuum plenum (via a short bellows visible in the bottom of Fig. 1) to remove hydrocarbons (methane) and noble gases that cannot be pumped by NEG modules.

All cavity surfaces are water cooled with passages tailored to the local surface power densities expected at full power CW operation. For example, the highest heat flux regions, on the sides of the nose, have closely spaced channels, with relatively high Reynolds number flow. In contrast, the anode end cap, a low power region, contains widely spaced, brazed on, cooling tubes with moderate Reynolds number flow.

As employed in other electron guns, the photo-emitting material is applied to a removable plug that can be replaced in-situ without breaking vacuum via a load lock. The load lock and initial plug design were provided by INFN/LASA and is not covered in this article. However, initial testing of the gun led to modifications to the plug design, that will be discussed in a later section.

The gun cavity is closed by a single 3 mm wide fusion weld (visible in inset (a) of Fig. 3) joining the anode end cap subassembly to the lower portion of the gun cavity. A narrow elevated rim on the end face of the cavity wall , as shown in inset (b) of Fig. 3, provides a high pressure contact to the copper portion of the anode end cap assuring minimal resistance to current flowing axially through the cavity. These design features allow the cavity to be opened (by grinding away the weld) and re-sealed (re-welded) multiple times should inspection and/or repair of the internal cavity surfaces be necessary.

IV. FABRICATION OF GUN SUBASSEMBLIES

As shown in Fig. 4, the gun is formed from five subassemblies: cathode end cap; nose; cavity wall; anode end cap and vacuum wall. All cavity structures are fabricated from OFE (UNS C10100) class 1 copper, or class 2 material when dimensions preclude availability of class l stock. Copper forgings for the gun cavity were inspected using a standard ultrasonic non-destructive examination (NDE) method to screen for voids and/or inclusions. The vacuum wall and the large flanges on the cathode and anode that jointly provide the required structural rigidity for the gun, are fabricated from 304 stainless steel plate and commercial 304 stainless steel vacuum fittings and tube. The beam pipe at the exit of the RF cavity is constructed from 316L tube and a 316LN vacuum flange to minimize the residual magnetic field at the cathode and along the beam path. The interior surfaces of all features are electropolished either before welding or, if accessible, after welding.

All vacuum joints are either electron beam (Ebeam) welded, Ebeam brazed or tungsten inert gas (TIG) welded. The internal surfaces of cavity parts that are to be joined by Ebeam welding are initially machined 'oversized' such that an extra 0.7 to 1.0 mm of material

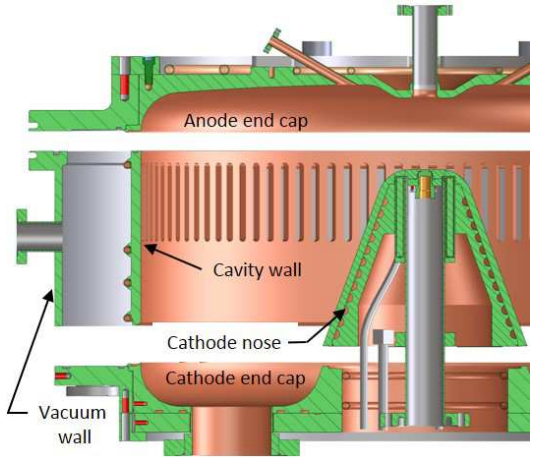

FIG. 4. VHF-Gun cross-section with subassemblies separated.

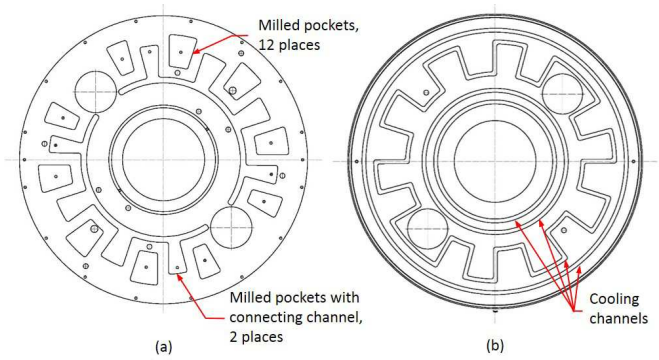

FIG. 5. (a) Cathode Backing Plate, (b) Cathode Inner Plate.

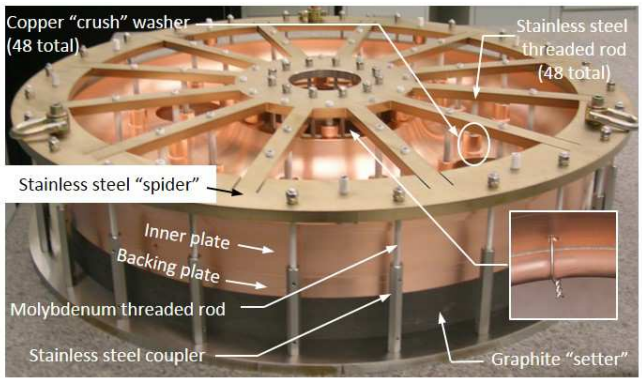

FIG. 6. Cathode end cap in brazing fixture.

remains. This extra material (or "material allowance") is removed after the parts are joined thus producing a smooth inner surface profile. An Ebeam braze joint between both anode and cathode end caps and their respective flanges, visible for the anode in inset (b) of Fig. 3, serve as vacuum seals only. Mechanical loads (pressure, thermal and gravity) on both cavity end caps are resisted by bolted connections.

An Ebeam welded/brazed final gun assembly was selected for its reliability and the ability to be re-worked without causing significant additional fabrication cost or delay. Secondly, fusing material using Ebeam techniques produces a very localized heat affected zone leaving the bulk of the material in a work-hardened state. This is especially important for assuring adequate pressure for good electrical contact between the anode end cap and the cavity wall. An added benefit is a significant reduction in the fixture complexity and preparation effort in comparison to furnace brazed construction.

A description of each subassembly follows.

A. Cathode End Cap

The cathode end cap subassembly is a water cooled structure formed by hydrogen furnace brazing two large circular copper plates, shown in Fig. 5. The internal surface of the cathode end cap inner plate is 'rough' machined leaving 0.8 mm of extra material to be removed after the brazing is complete. Water passages machined into the back of the inner plate are sealed by a backing plate. The specified machining tolerances assure that mating surfaces have at most a 50 μm braze gap. To provide adequate contact pressure for good braze filler wetting, large shallow pockets are machined into the backing plate between water channels thus reducing the contact area between plates.

A brazing fixture, visible in Fig. 6, was constructed using molybdenum 'draw' rods to generate a compressive load between top and bottom plates via differential thermal expansion. Copper 'crush' washers on stainless steel studs at the point of contact (on the inner plate surface) prevents the cavity surface from permanently deforming, locally, beyond the 0.8 mm machining allowance. A 50 mm thick graphite 'setter' plate between fixture's base plate and brazement assures that the assembly remains flat. Cooling tubes are brazed to the inner bore of the end cap in the same operation. To hold these tubes in place for brazing, short lengths of stainless steel wire are inserted into small holes drilled into the plate on either side of the tube at multiple points along its path. These wires are then peened into place, wrapped over the tube and twisted tightly to draw the cooling tube against the surface, as shown in the inset in Fig. 6. Braze filler paste is applied to form a fillet at the wall-tube interface.

A cross-section of the CAD model for the completed end cap is shown in Fig. 7. Vacuum flanged ports for the RF power couplers are fabricated by Ebeam brazing a heavy wall copper tube to a modified 6.75" Conflat flange, refer to the inset in Fig. 7. This operation retains the stainless steel knife edge vacuum feature while presenting a copper face for a low resistance electrical connection across the joint. The neck of the completed coupler port is subsequently Ebeam welded to the inner

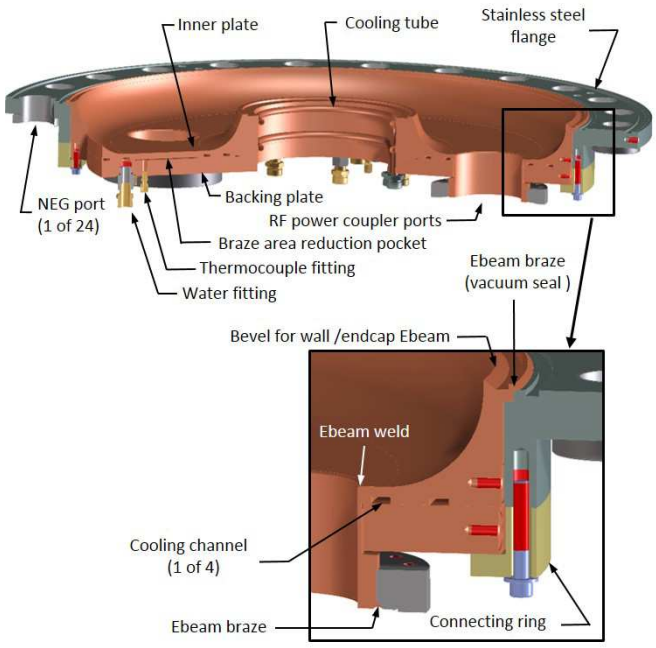

FIG. 7. Cross-section of the VHF-Gun cathode end cap.

plate of the end cap brazement.

The connection between vacuum wall and the cathode is achieved by bolting the copper portion of the end cap to a stainless steel "connecting ring" that is also fastened to an approximately 1 m OD stainless steel flange. The twenty-four 41 mm ID Conflat-flanged ports, TIG welded to this flange, are provided for mounting NEG pump modules. With the end cap securely bolted together, the outer rim of the cathode brazement is Ebeam brazed to the stainless flange providing a vacuum tight seal, as shown in the inset in Fig. 7.

B. Cavity 'Nose'

The re-entrant cavity 'nose' subassembly houses the cathode plug and 'bucking' solenoid. A CAD model of this subassembly is shown in Fig. 8 with a cross-section of the component subassemblies shown in Fig. 9. A gold plated 316 stainless steel canted-spring-ring, located in a groove in the copper 'receiver' disk, see the inset in Fig. 9 (b), provides the electrical contact between the plug and the gun cavity. The precision ground 316L stainless tube 'central tube' provides a UHV environment for moving the cathode plug from the load lock to the gun. Additionally, the tube's OD serves as an accurate, concentric, locating feature for the 'bucking' solenoid. This solenoid produces a small field (up to 66 G) at the cathode face to counter stray magnetic field from a focusing solenoid typically located immediately downstream of the VHF-Gun.

As evident in Fig. 9, the nose is assembled from the central tube subassembly and a separate concentric cone brazement. The dimensional tolerance of cathode receiver disk is 25 to 50 μm, depending on the specific feature. The exacting internal feature tolerances combined with the relatively delicate 2 mm thick internal protrusion, that shields the canted spring from the accelerating gap, make machining these features as part of the large outer cone difficult and risks ruining a large, expensive part. The two part assembly selected allows the receiver disks' internal profile to be machined and inspected separately thus making these tasks relatively easy. To assure that the cathode plug surface is exactly coplanar with the end of the nose, a 4 mm wide annular surface on the receiver disk face surrounding the cathode plug opening was machined to final thickness. The remaining surface is left with about 1 mm of extra material that is removed after the disk is joined to the cone.

The cathode receiver disk is joined to the central tube by an Ebeam braze that fuses the perimeter of the disk to the OD of the central tube, see Fig. 9 (b). This joint is tested for vacuum integrity before proceeding with the nose assembly. A stainless steel 'mounting' disk fastens to the receiver disk using 3 small, vented, socket-head cap screws. The function of the mounting disk is to center the cathode plug accurately and to provide a durable stop for the plug during insertion in the gun. This mounting arrangement, as well as the load lock design, is a copy of the INFN/LASA design[20]. The initial cathode plug, typically machined from sintered molybdenum, was taken from a FNAL modification to a INFN/LASA design[21].

Bench testing of the FNAL plug at LBNL revealed that repeated plug insertions caused deformation, and eventually failure, of the canted-spring-ring. Three small modifications to the plug design eliminated the problem, refer to Fig. 10. The first two changes were adding a radius to the leading edge and reducing the conical entrance angle from 30 to 20 degrees. The third change was reducing the plug OD by 230 μmin in the area where the plug contacts the canted-spring-ring.

The sides of the nose absorb the highest power density of any surface in the gun, as will be discussed in Section VII. To dissipate this heat, two parallel spiral cooling channels are milled into the surface of the inner cone. A close fitting outer cone blocks the majority of flow from bridging adjacent passages. Complete isolation of adjacent cooling passages is not expected or necessary to achieve the required heat dissipation. Braze joints, using a palladium-copper-silver alloy (PalCuSil15), between the flat internal mating surfaces at the top (narrow end) of the cones and on a short precisely machined cylindrical segment at the base of the cones, see Fig. 9 (a), provide a hermetic seal. Both braze joints serve to isolate water from air only.

To complete the nose assembly, the central tube subassembly is placed flush with the nose surface and a 6 mm deep Ebeam fusion weld is made between the close fitting cathode receiver disk and precisely bored cone. A helium leak check is performed to verify the integrity of the weld. The extra material on the outer cone and re-

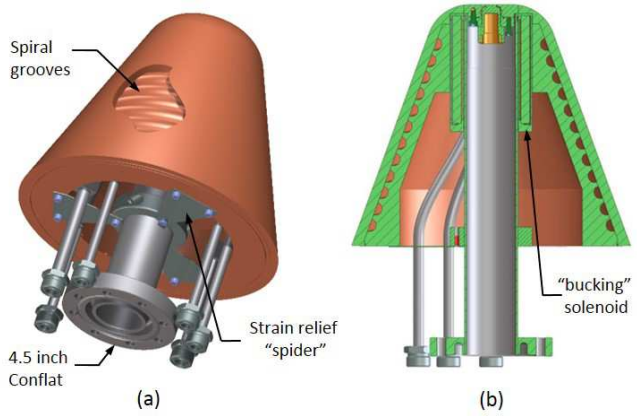

FIG. 8. (a) Cathode 'nose' subassembly, (b) Cathode nose subassembly in cross-section.

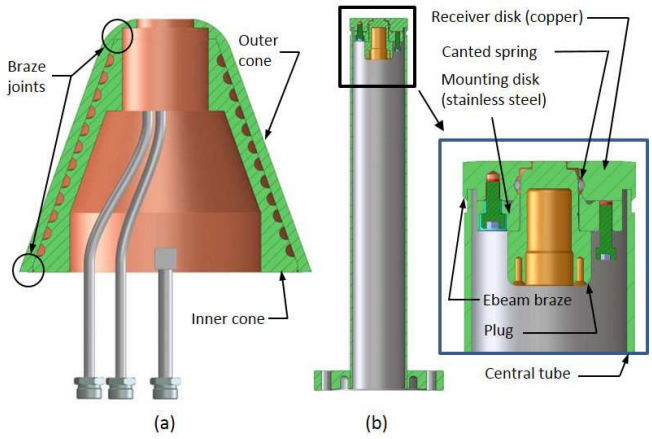

FIG. 9. (a) Cross-section 'nose' cone brazement, (b) Cross-section of central tube subassembly.

ceiver disk is removed in a subsequent operation. An internal 'spider' assembly, see Fig. 8 (a), is clamped to the central tube and screwed to the inner cone to prevent an inadvertent transverse force from deforming the nose tip or central tube. The solenoid is then installed and a modified 4.5 inch Conflat flange is TIG welded to the end of the central tube.

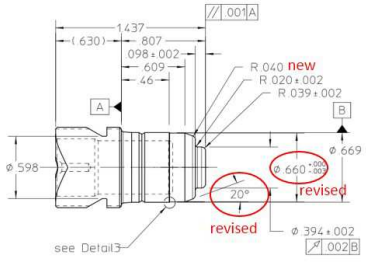

FIG. 10. LBNL revision to the cathode plug design.

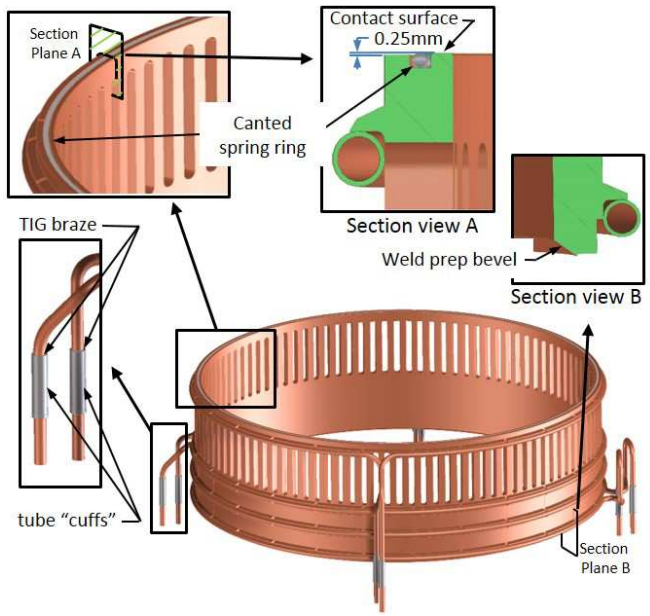

FIG. 11. Cavity wall subassembly with section views of top and bottom profiles.

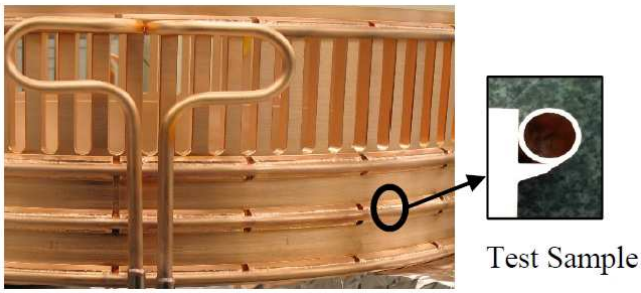

FIG. 12. Fusion weld of cooling tube to cavity wall.

C. Cavity Wall

The cavity wall is machined from a 1/4-hard forged copper cylinder. An array of 104, 11 mm wide × 12 mm deep × 110 mm long slots are milled through the wall to provide a large pumping conductance from cavity to plenum ($\sim 7 \times 10^6$ l/s for hydrogen and $\sim 2 \times 10^6$ l/s for CO). Cooling water flowing through tubes fused to the exterior of the wall, remove the approximate 3 W/cm^2 heat flux while limiting the temperature rise to about 40^{o}C, as noted in Section VII. Refer to the CAD model of the cavity wall assembly in Fig. 11. Through trial and error, a ledge shaped feature was found that, when machined into the wall surface, permits a reliable 1.0 to 1.5 mm deep TIG fusion weld between the tube and cavity wall without breeching the cooling tube wall. A picture of the completed cavity wall subassembly is shown in Fig. 12. A sectioned cavity wall braze test specimen is inset in this figure.

A 3 mm wide × 0.25 mm tall rim is machined into the

the top (anode side) surface of the cavity wall. Once the cavity is assembled, the face of this rim bears against a flat surface on the anode end cap to form the primary high current RF contact. Immediately adjacent to the rim is a square groove for a a gold plated stainless steel canted-spring-ring that serves as the secondary (back-up) electrical contact, see Fig. 11 Section view A. Stainless steel material was selected for the spring ring to withstand the elevated vacuum baking temperatures of up to 220^{o}C. A 20 μm gold coating on the spring (equivalent to 4 skin depths at 186 MHz) provides a low resistance RF path between surfaces.

A deep chamfer is machined into the base of the cavity wall that matches the bevel on the upper surface of the cathode end cap, see Fig. 11 Section view B. As will be evident in Section VI, the angle of this chamfer facilitates an Ebeam directed parallel to the joint, unobstructed by the cathode nose.

The assembly sequence of the cavity wall begins with attachment of the cooling tubes to the wall followed by TIG brazing stainless steel 'cuffs' to the tubes using a gold-copper filler (35Au/Cu) over the copper tube ends, shown in Fig. 11. The stainless cuffs are welded to the cathode flange during the gun assembly. The copper tubing extends through the cuffs to the exterior of the gun for connection to the water cooling system. This coaxial tube arrangement is consistent with the design rule of no brazed or welded water/vacuum joints and has the added benefit of providing a high reliability all stainless steel fusion weld vacuum as the final step.

D. 'Anode' End Cap

In contrast to the cathode, the anode end cap shown in Fig. 13, is constructed by TIG brazing copper cooling tubes, using a palladium-copper-silver (PalCuSil-10) alloy, to the exterior surface of a machined copper plate. This operation anneals the material in the vicinity of the braze only, leaving the bulk of the copper in a work-hardened state. This is important since annealed copper may yield during gun assembly resulting in a loss of adequate electrical contact with the cavity wall.

The exterior surface (air-side) of the copper anode plate is ground to be coplanar with the surface of the adjacent stainless steel flange. The structural support for the copper anode plate is provided by the flange through a bolted connection to a stainless ring that overlaps both surfaces, see Fig. 13. Subsequently, the vacuum seal for anode, as with the cathode end cap, is formed by fusing a 3 mm tall copper ledge, machined into the end cap, with the interior surface of the adjacent stainless steel flange, see Fig. 13 Section A-A. With the flange and tubes attached, the anode's copper inner (cavity side) surface is finish machined to final dimensions to within a profile tolerance of 50 μm over the central 15 cm diameter. Surface finish in this region is held to better than 0.4 μm (16 micro-inch) RMS.

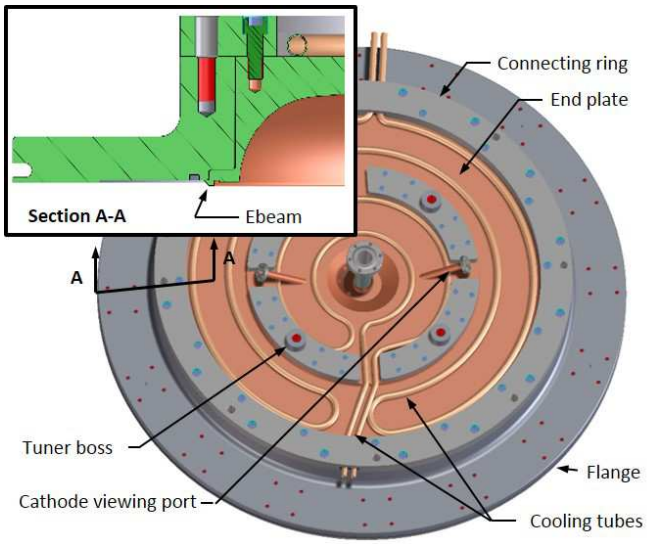

FIG. 13. Anode subassembly.

Figure 13 also shows the two diametrical opposed cathode inspection viewports. These ports can be used either for inspecting the proper insertion of the cathode plug in the nose tip housing, or as alternate laser port for illuminating the cathode at a grazing (30 degree incidence) angle. In normal operation the cathode is illuminated quasi-perpendicularly by a mirror located in the beamline downstream of the gun. The viewports are fused-silica with a transparent-conductive coating of indium-tin oxide to avoid charge build-up and a possible consequent vacuum leak due to a 'punch-through' arc through the window.

E. Vacuum Wall

The vacuum wall subassembly is a conventional TIG welded UHV component. The main body of the subassembly consists of a rolled and welded 304 stainless steel cylinder welded to a flange machined from 304 stainless steel plate stock. With the main flange in place, the weldment is helium leak checked and then electropolished. Holes are machined in the cylinder to accept six 2.75" and one 8" Conflat flanged ports. The small ports are allocated for ion gauges, a residual gas analyzer, and a rough vacuum pumping station. The larger port, as previously mentioned, is used for the 300 l/s ion pump. After these ports are welded in place the assembly is once again leak checked. Key design details of the fabrication of this subassembly are shown in Fig. 14.

With welding complete, the flange on the anode end of the assembly is machined flat to within 0.13 mm, see Fig. 14 Detail 2. The cathode end of the assembly is machined parallel to the flange (anode end) face to within 50 μm. A 0.4 mm step is machined into the end of the cathode end of the cylinder to help locate the vacuum

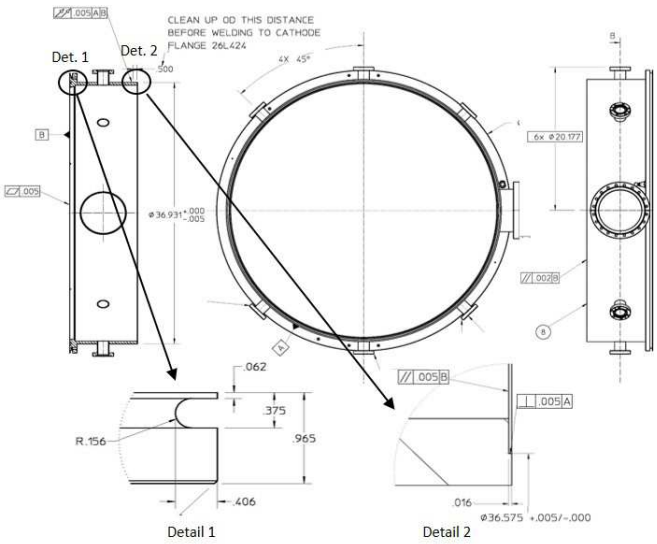

FIG. 14. Excerpts from vacuum wall fabrication drawings.

wall on the cathode flange. The machining tolerance (+/- 0.13 mm) on the inside diameter the step, combined with an equal tolerance on the locating step of the cathode flange, assures that the vacuum wall is concentric to the cathode within 0.26 mm. A 10 mm deep weld prep is machined into the perimeter of the flange to allow the gun to be disassembled and re-assembled repeatedly.

V. GUN ASSEMBLY

To initiate the gun assembly, the base of the cavity nose cone is Ebeam welded to the raised face on the cathode end cap inside diameter (visible in Fig. 4), providing both the vacuum seal and mechanical connection, see Fig. 15. The vacuum wall assembly is then seated on the cathode end cap flange and a continuous vacuum sealing Ebeam weld is made at the inside diameter. An Ebeam skip weld on the outside diameter is then added to provide mechanical strength to the joint. In a subsequent operation, a 6 mm deep Ebeam weld joins the cavity wall to the cathode end cap. The components, shown mounted to the rotary stage in Fig. 16, are tilted to allow the downward pointing electron beam to pass by the nose and strike the base of the cavity wall parallel to the cathode/cavity wall interface.

After welding, the internal surfaces of the cathode end cap, the nose and the base of the cavity wall are machined as a unit to final dimensions. A profile tolerance of better than 125 μm is maintained for the cavity wall and cathode end cap inner (cavity side) surfaces with a 50 μm tolerance specified for the nose. Surface finish of the nose face and shoulder is held to better than 0.4 μm (16 micro-inch) RMS. Following machining, a helium leak test is performed to assure that no leaks were generated by material removal from the weld regions.

FIG. 15. Cathode end cap and nose after Ebeam welding.

FIG. 16. Cavity wall secured to cathode for Ebeam welding.

As will be discussed in Section VII, the VHF-Gun's frequency is predominantly determined by the distance between the cathode nose and anode. Removing material from the anode rim reduces the gap thereby increasing the capacitance of the nose-anode gap and decreasing the frequency. Therefore the desired gun frequency is achieved by reducing thickness of the rim of the anode end cap that contacts the cavity wall and the anode flange mating surface equally, refer to Fig. 3. Finite element analysis was employed to calculate the expected natural frequency shift due to material removal from the anode as well as the expected frequency at operating conditions (including both vacuum and thermal effects). The frequency was adjusted in two machining cycles using

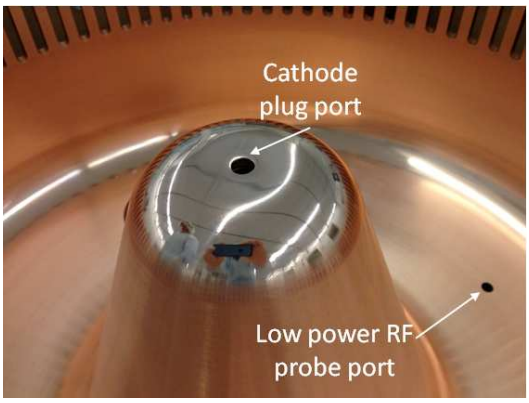

FIG. 17. Cathode nose after mechanical polishing.

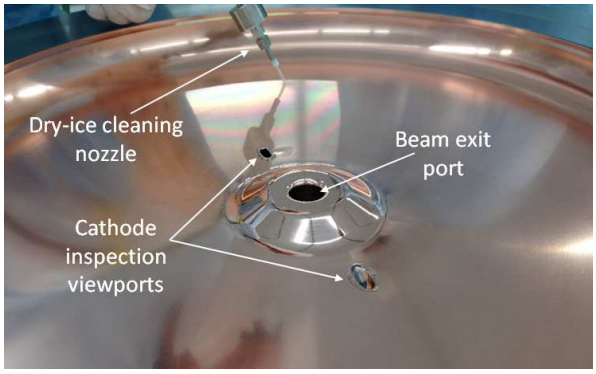

FIG. 18. Dry ice cleaning of anode surface.

a CNC vertical turret lathe. As a first step, approximately half of the required material was removed. The cavity was then re-assembled (by mechanical clamping) and a frequency measurement was made to verify the frequency-to-height sensitivity. Once this sensitivity was confirmed, a final machining pass was executed to bring the cavity to the target frequency.

Flatness of the anode/cavity wall RF contact surfaces to better than 30 μm was achieved by successive 'light' cutting passes using a vertical turret (VTL) and conventional tooling. To verify the quality of the contact, a thin layer of Dykem Blue layout fluid was applied to the cavity wall contact surface, and the anode end cap was immediately clamped in place. By reopening the cavity and observing the uniformity of the Dykem distribution on the anode surface it was possible to verify that contact was achieved over the entire circumference. As designed and fabricated, when the anode flange is mated to the lower cavity the anode end cap will rest on the cavity wall while a 13 to 25 μm gap will exist between the mating vacuum wall and anode flanges. Subsequent clamping of the these flanges in conjunction with the vacuum load on the anode end cap assures that good RF contact between the cavity wall and anode is achieved. As noted previously, a canted spring ring adjacent to the raised contact surface on the cavity wall, see Fig. 3, is provided as a redundant contact and is capable of carrying the full wall current in the event that the primary connection is lost.

After the requisite cavity frequency is achieved, the central portions of the cathode nose and anode are mechanically polished, using extra fine silicon-carbide paper followed by 3 μm diamond paste on felt, to produce the mirror finish shown in Fig. 17. Following mechanical polishing the interior cavity surfaces are given a UHV cleaning treatment consisting of a hot detergent wash followed by a low conductivity water rinse. UHV cleaning is followed by a light etch using a chromic acid solution and then a final hot, low conductivity(>10 Mohm-cm), water rinse. The etch and rinse steps remove particulates that may have adhered to the surface during polishing. All exterior surfaces are cleaned so as to be compatible with subsequent introduction of the gun into a cleanroom environment. With the gun in a class 1000 cleanroom, the interior surfaces are subjected to dry-ice cleaning (DIC) using supercritical extraction grade carbon dioxide and a hand-held nozzle, see Fig. 18. Once all surfaces are cleaned, the anode end cap is placed onto the lower cavity, all ports are sealed and the gun is removed from the cleanroom.

Final assembly of the gun consists of aligning the anode to cathode bores and welding the anode end cap to the lower cavity at the vacuum wall. To assure accuracy, the pre-assembled gun is placed on a coordinate measuring machine (CMM), and with a filtered dry-nitrogen gas purge in place, a precisely machined alignment plug is inserted into the cathode nose through the center tube subassembly in the cavity nose. A cylindrical portion of the plug extends beyond the nose face towards the inside of the cavity providing a surface for the CMM's touch probe to safely reach through the anode bore (beam exit port) and locate the cathode bore without contacting the cathode nose surface directly. Using the CMM as a guide, the anode end cap is driven into alignment with the cathode. Once the cathode and anode bores are aligned to within 15 μm, the anode end cap is clamped in place and the final vacuum seal is made by TIG welding the thin (2 mm) lip on the vacuum wall flange to a corresponding lip on the anode end cap flange, see Fig. 3 inset (a). Initially four equally spaced tack-welds are made in opposing pairs and the alignment is re-checked. Provided that the alignment is still within tolerance a small fusion weld is symmetrically applied around the full circumference and the alignment is given a final check followed by a through helium leak check of all joints.

VI. ANCILLARY COMPONENTS

A. RF Power Couplers and Probes

RF energy is transferred into the VHF-Gun via two identical water-cooled high-power loop couplers capable

of up to 60 kW CW RF power each, see Fig. 19. The loop couples with the magnetic component of the RF field in the cavity and provides a 50 ohm termination on a 4-1/16 inch coaxial waveguide when both couplers are driven in phase with the same power. The two power couplers are mounted to symmetrically located ports in the cathode end cap, see Fig. 2. This configuration helps minimize dipole field distortion due to the break in axisymmetry associated with the insertion of the RF couplers. Each loop is individually tuned (rotated) to produce a coupling constant $\beta = 0.5$, or an S11 parameter at resonance of 0.333, for a total coupling factor of 1.

The coupler body, loop and 'hub' are fabricated from OFE copper and joined by vacuum furnace brazing using 35Au/Cu alloy, see Fig. 20. In the same braze operation, the stainless steel water cooling block is brazed to the ends of the loop, see inset (e) of Fig. 20, to form a water tight seal. An air gap between the block and body allows helium leak checking of the vacuum braze joints between loop tube and body and assures that a single joint failure cannot admit water into the vacuum volume. The completed hub/loop/water block brazement is joined to Conflat flanges (evident in Fig. 20 insets (b) and (c)) at either end by Ebeam brazing.

The center conductor subassembly is an Ebeam welded assembly consisting of a short section of thin-wall copper tube and a relatively thick-wall adapter penetrated by 8.7 mm through hole, see Fig. 20 inset (d). A final Ebeam weld of the center conductor to the hub completes the assembly of the coupler assembly. After assembly, all of the vacuum exposed surfaces are coated with a titanium nitride (TiN) layer of few hundred nm to reduce secondary electron emission and thus suppress multipacting.

A custom 'nut' and Belleville spring washer trapped inside the inner conductor are used to secure the center conductor of the coupler to a threaded stud mounted to the center conductor of the coaxial RF distribution line (not shown). The nut is driven by 6.4 mm hexagonal rod inserted through the hole in the hub, see Fig. 20 inset (a). The spring washer helps assure that the nut does not work loose due to thermal cycling over time. The coupler body (outer conductor) is joined to the gun by a rotatable Conflat flange. The vacuum seal and RF connection are made by a custom copper gasket, see Fig. 20 inset (b). A similar gasket serves the same function for the connection between the coupler and coaxial RF distribution line.

A 4 inch nominal commercial UHV compatible ceramic window (Toshiba E4278) provides the vacuum barrier between the gun cavity and the air insulated coaxial RF waveguide. The geometry of RF window area is presently being revised to eliminate line-of-sight between the ceramic surface and the cavity interior. This modification should eliminate the possibility of charge build-up (with consequent arcing) on the ceramic by field emitters on the cavity wall.

An addition, two small sensing loops located on the cathode end cup wall are provided to produce a power of approximately 1 watt at the full cavity excitation level for closed-loop feedback and monitoring.

FIG. 19. The Coaxial RF coupler. The gold and dark–red coloration is due to the titanium nitride coating.

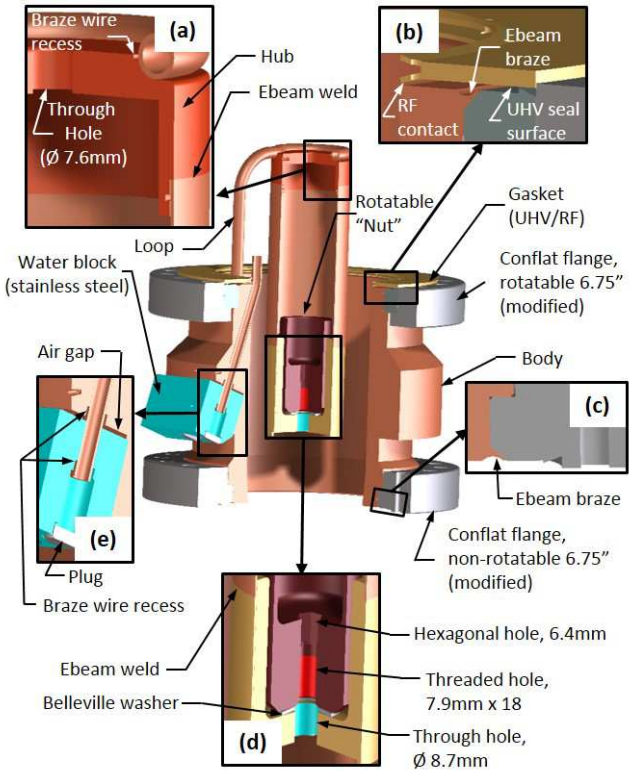

FIG. 20. Coupler assembly with a quarter section cut-out to shown the internal structure.

B. Tuner

The natural frequency of the gun is actively maintained at the fixed driver frequency with ~ 1 kHz accuracy during operation by adjusting the nose-to-anode accelerating gap. This adjustment is achieved by elastically deform-

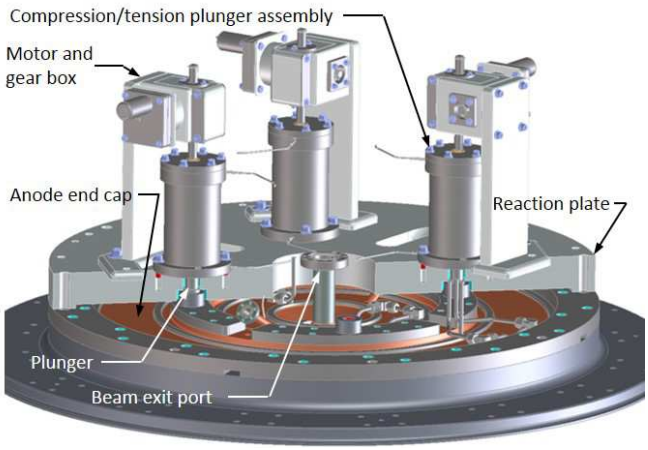

FIG. 21. Model of proposed production tuner units (3 of 4 shown). Note the reaction plate is sectioned to show the connection to anode end cap.

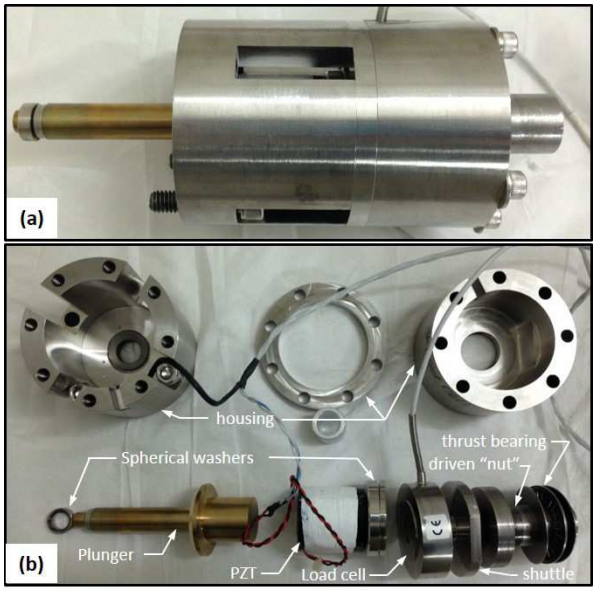

FIG. 22. (a) Prototype tuner compression plunger assembly. (b) Disassembled plunger assembly.

ing the anode end cap through application of a compressive force at four equally spaced locations on the exterior of the end cap. A CAD model, Fig 21, containing the proposed bi-directional (compression and tension) production units for LCLS-II, illustrates the arrangement of tuner elements on the gun face. A picture of the prototype compression plunger assembly, in current use on the VHF Gun, is shown in Fig 22 (a). The internal components are shown disassembled in Fig 22 (b). The force is generated by a combination motor driven screw actuator (nut and threaded shuttle pair) and a lead zirconate titanate (PZT) piezoelectric ceramic actuator contained in 'tuners' bolted to a ~ 50 mm thick aluminum reaction plate attached to the exterior edge of the anode. The motor-driven nut, PZT and a 13 kN load cell are arrayed in series to transmit a measured compressive force to a plunger in contact with the anode surface.

The action of the four independent tuner drive units is coordinated by limiting the amplitude of the force step change and equilibrating the applied compressive forces before proceeding to the next load step. Coarse adjustment is provided by a low power 1/30th HP DC gear motor attached to a 30:1 worm and pinnion gearbox. Fine adjustment is provided by the high voltage PZT (Piezomechanik HPSt1000/35-25/40), which is limited to an effective displacement of < 40 μm and rated for 20,000 N maximum force generation. Each tuner is capable of delivering up to 10,000 N to the face of the anode. In operation the force required is less than 4000 N per tuner. The measured frequency sensitivity to applied force is 19 Hz/N per tuner and the measured tuner displacement to frequency sensitivity is 540 kHZ/mm.

VII. THERMAL AND STRESS ANALYSIS

While the main focus of the present article is the mechanical design and fabrication of the VHF-Gun, this effort was preceded by an iterative RF cavity design and engineering analysis effort. A brief summary of the extensive thermal and structural analysis of the 'as-built' VHF-Gun is provided below.

A vector plot of the surface power densities for the final cavity shape, calculated using POISSON/SUPERFISH, is shown in Fig. 23. Empirical formulas for convective heat transfer coefficients were used in conjunction with finite element analysis (FEA) using ANSYS to determine cavity temperatures and deformation during operation. These coefficients were applied directly to the surfaces of cooling channels formed from milled passages. Where cooling tubes are bonded (welded or brazed) to surfaces, a local region surrounding the tube was modeled separately to determine an equivalent convective heat transfer coefficient to be applied to a representative surface on a simplified FEA model of the full gun. An example of this process, as applied to the cavity wall, is illustrated in Fig. 24 with the (a) portion showing the boundary conditions applied to two representative (1.7 degree slice) models of the cavity wall. The resultant temperature contours contained in Fig. 24 (b) show that the selected heat transfer coefficient applied to the simplified wall section results in temperature distribution that is nearly identical to the more physically accurate model.

Given the axisymmetric cavity geometry, an FEA model of a 6 degree radial slice adequately represents the gun. The thermal model incorporates heat loads, convective boundary conditions and the appropriate material properties to determine the cavity temperature dis-

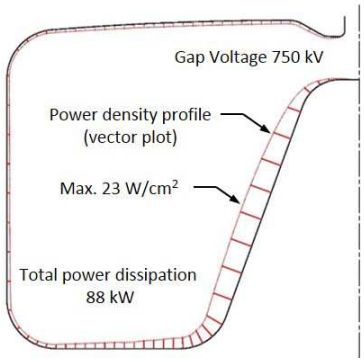

FIG. 23. Surface power densities calculated by POISSON/SUPERFISH for the VHF-Gun for full power operation .

tribution, shown in Fig. 25. Deformation due thermal expansion and external pressure (vacuum) is shown in Fig. 26. As mentioned previously, the resonant frequency of the gun cavity is a strong function of the gap between the anode and cathode nose. Frequency control of the VHF-Gun is achieved by pushing against four equally spaced points on the anode surface to modulate this gap length. By design, the structurally weakest portion of the gun is the anode end cap. Finite element analysis was used to evaluate the tuner force required to achieve a reasonable tuning range (∼120kHz) and the resulting peak stress in the structure. The four-fold symmetry of the anode/tuner geometry allowed the use of a quarter section FEA model, see Fig. 27. Note the maximum stress in the copper is 45 MPa, safely below the yield point (117 MPa) for work-hardended copper but above the elastic limit (34 MPa) of fully annealed OFE copper. The end cap geometry was determined by an iterative process of balancing, tuner force, end cap stress, sensitivity to atmospheric pressure and temperature rise.

VIII. CONCLUSIONS AND FINAL CONSIDERATIONS

The mechanical design rationale and the fabrication techniques used for the VHF-Gun, the CW high-brightness high-repetition rate electron gun developed at LBNL in the framework of the APEX experiment, and for its subsystems have been described.

To date, the VHF Gun has already operated successfully and reliably at the nominal parameters (750 keV energy and 1 MHz pulse repetition rate with a charge per bunch of several hundred pC) for an integrated period of a few years, and all design goals in Table I and Section II have been demonstrated with margin. A detailed description of the gun performance can be found elsewhere[10]. Additionally, dark current has been fully characterized[22] and dramatically reduced by dry-ice cleaning combined with careful mechanical polishing of the central cathode and anode areas. Extensive tests demonstrated the capability of Cesium Telluride (Cs_2Te) cathodes, produced

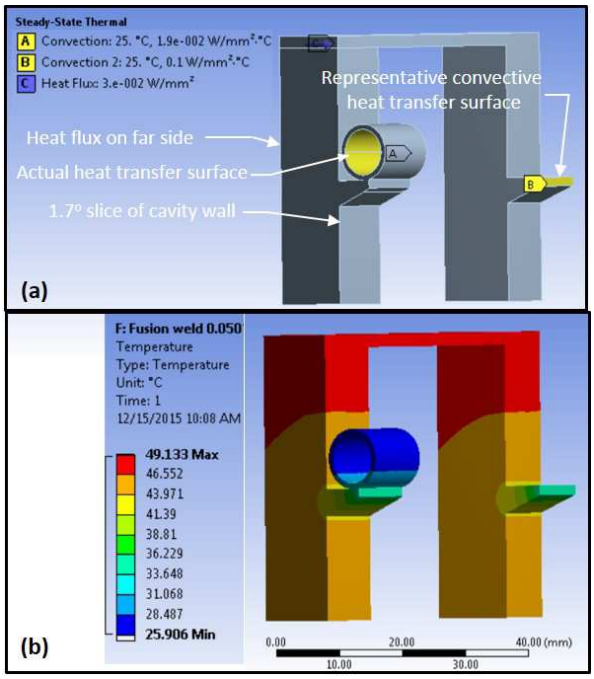

FIG. 24. (a) Boundary conditions for an FEA model containing both a physically accurate and simplified rendering of the cavity wall with convection coefficients adjusted to give equivalent results. (b) Resultant temperature contours.

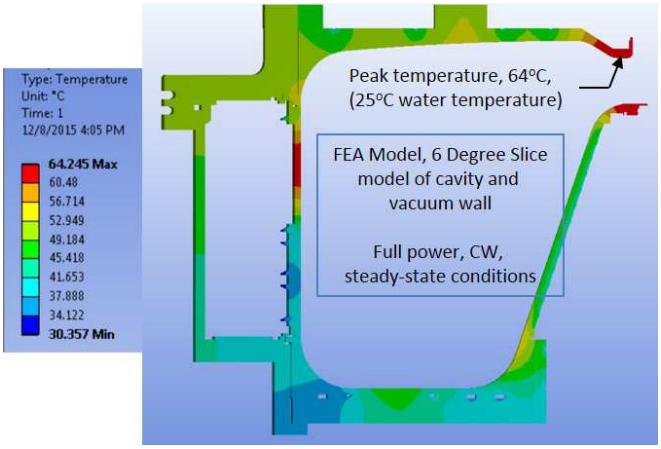

FIG. 25. Thermal contours from FEA modeling of a 6 degree slice of the VHF-Gun.

by INFN/LASA, to operate at the challenging regime imposed by X-ray FEL applications[23].

A second generation VHF Gun, being developed at LBNL for the LCLS-II project at SLAC, incorporates some improvements on the original design. Primarily these consist of three items. The first being replacing the brazed-on cooling tubes with milled cooling channels in the anode end cap. As presently envisaged, these cooling channels will be capped by Ebeam welded covers. The advantage is enhanced cooling and a reduction in the thermal expansion of the anode with a concomitant

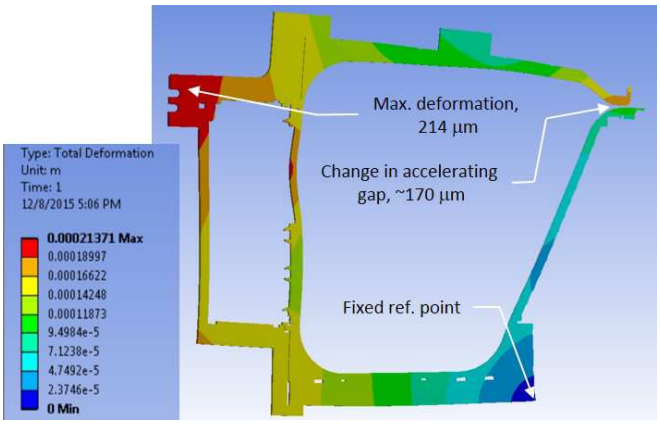

FIG. 26. Contour plot of the vector sum of radial and axial deformation of the VHF-Gun due to thermal expansion and external (atmospheric) pressure.

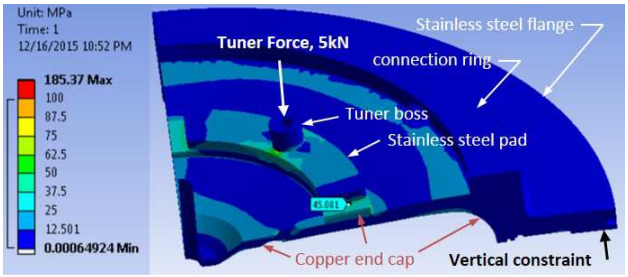

FIG. 27. Contour plot of the von Mises equivalent stress in the anode due to a 5 kN tuner force and atmospheric pressure, in MPa.

reduction in the frequency excursion that occurs during warm-up, the first ~ 30 minutes of operation. The lower temperature will have the added benefit of lowering the residual gas pressure during operation. The second item is a bi-directional tuner that provides either tensile or compressive force on the anode to raise or lower the cavity frequency, respectively. This tuner utilizes the same basic design concept and commercial components as the original unit but with a doubling of the PZT's and load cells to provide for bi-directional load and force feedback. This change increases the tuning range of the system. The third item is a small change in the position of the NEG pumping ports on the cathode end cap. Moving these ports slightly radially outboard provides the space needed for installation of SAES NexTorr Ion/NEG pumps. The use of a mix of distributed small NexTorr and CapaciTorr NEG units eliminates the need for the large sputter ion pump used with the present VHF-Gun. Eliminating the large ion pump allows the VHF Gun to be situated much closer to the floor as required in the LCLS-II installation. These changes should improve performance, operating flexibility and the compatibility of the VHF Gun for use with LCLS-II or other similar facilities.

ACKNOWLEDGMENTS

The authors want to thank David Dowell, Erik Jongewaard, Rick Kraft, Ali Nassiri, Robert Rimmer, Vadim Veshcherevich and Steven Virostek for reviewing the gun design, the LBNL mechanical shop technicians for the gun fabrication, and Berkeley Lab Director, for supporting the initial phase of the project. The authors wish to thank the Director of the Office of Science of the US Department of Energy for funding this work.

[1] A. Belkacem, *et al.*, Synchrotron Radiation News, Vol. 20, Issue 6, 2007, p. 20.
[2] J. Corlett, *et al.*, Synchrotron Radiation News, Vol. 22, Issue 5, 2009, p. 25.
[3] R. P. Walker, *et al.*, Proceedings of the 2009 Particle Accelerator Conference, Vancouver, BC, Canada, May 4–8, 2009, p 1141.
[4] J. Bisognano, *et al.*, Proceedings of the 2009 Particle Accelerator Conference, Vancouver, BC, Canada, May 4-8, 2009, p 109.
[5] See for example, E. Arenholz, *et al.*, *Toward Control of Matter: Basic Energy Science Needs for a New Class of X–ray Light Sources. Proceedings of the Science for a New Class of Soft X-ray Light Sources Workshop*, Berkeley, CA, October 8-10, 2007; LBNL Report LBNL–1034E, September 24, 2008, (available at http://www.osti.gov/scitech/biblio/941167).
[6] J. Galayda, Proceeding of IPAC14, Dresden, Germany, June 2014, p. 935.
[7] F. Sannibale, D. Filippetto, and C. F. Papadopoulos, Journal of Modern Optics, 58:16, 1419–1437.
[8] J. Staples, F. Sannibale and S. Virostek, *VHF-band Photoinjector* CBP Tech Note 366, Oct. 2006, LBNL–1003792 (available at https://publications.lbl.gov/publication_search).
[9] K. Baptiste, J. Corlett, S. Kwiatkowski, S. Lidia, J. Qiang, F. Sannibale, K. Sonnad, J. Staples. S. Virostek, and R. Wells, Nuclear Instruments and Methods for Phys. Research A 599, 9 (2009).
[10] F. Sannibale, *et al.*, Phys. Rev. ST Accel. Beams 15, 10351 (2012).
[11] F. Sannibale, *et al.*, Proceeding of IPAC14, Dresden, Germany, June 2014, p. 727.
[12] D. Filippetto, *et al.*, Proceeding of IPAC14, Dresden, Germany, June 2014, p. 730.
[13] D.H. Dowell, I. Bazarov, B. Dunham, K. Harkay, C. Hernandez-Garcia, R. Legg, H. Padmore, T. Rao, J. Smedley, and W. Wan, Nuclear Instruments and Methods for Phys. Research A 622, 685 (2010).
[14] T.M. Huang, CBP Tech Note 393, Dec.1, 2008, LBNL–1003794 (available at https://publications.lbl.gov/publication_search).
[15] J. Staples, CBP Tech Note 395, Apr. 2007, LBNL–1003793 (available at https://publications.lbl.gov/publication_search).
[16] J. Staples, G. Huang, and R. Wells, CBP Tech Note 378, July. 2007, LBNL–1003795 (available at https://publications.lbl.gov/publication_search).
[17] J. Staples, CBP Tech Note 379, August. 2007, LBNL–1003796 (available at https://publications.lbl.gov/publication_search).
[18] S. G. Liu, T. M. Huang, and J.Q. Xu CPC (HEP & NP), 2011, 35(9), p. 865-869.
[19] S. Lederer, P. Manini, Private communications.
[20] D. Sertore, S. Schreiber, K. Floettmann, F. Stephan, K. Zapfe, and P. Michelato, Nucl. Instrum. Meth. A 445 (2000) 422–426.
[21] FNAL drawing 4906.250-MC-459528.
[22] R. Huang, D. Filippetto, C.F. Papadopoulos, H. Qian, F. Sannibale, and M. Zolotorev, Physical Review Special Topics - Accelerators and Beams 18, 013401 (2015).
[23] D. Filippetto, H. Qian, and F. Sannibale, Applied Physics Letters 107, 042104 (2015).